Shock Waves (1996) 6: 183–195

Shock Waves

A numerical investigation of transient detonation in granulated material

K. A. Gonthier, J. M. Powers

Department of Aerospace and Mechanical Engineering, University of Notre Dame, Notre Dame, Indiana 46556-5637, USA

Received 4 August 1995 / Accepted 17 February 1996

Abstract. A two-phase model based upon principles of continuum mixture theory is numerically solved to predict the evolution of detonation in a granulated reactive material. Shock to detonation transition (SDT) is considered whereby combustion is initiated due to compression of the material by a moving piston. In particular, this study demonstrates the existence of a SDT event which gives rise to a steady two-phase Chapman-Jouguet (CJ) detonation structure consisting of a single lead shock in the gas and an unshocked solid; this structure has previously been independently predicted by a steady-state theory. The unsteady model equations, which constitute a non-strictly hyperbolic system, are numerically solved using a modern high-resolution method. The numerical method is based on Godunov's method, and utilizes an approximate solution for the two-phase Riemann problem. Comparisons are made between numerical predictions and known theoretical results for 1) an inert two-phase shock tube problem, 2) an inert compaction wave structure, and 3) a reactive two-phase detonation structure; in all cases, good agreement exists.

Keywords: Two-phase flow, Shock to detonation transition, Non-strictly hyperbolic systems, Approximate Riemann solvers

1 Introduction

There has been considerable research during the past two decades addressing the evolution of detonation in granulated energetic material. Much of this research has been motivated by concerns over the accidental detonation of damaged high-explosives or propellants in response to mechanical impact or thermal insult. Here, damaged material refers to cast solid material which has been inadvertently fractured; thus, local granulated regions exist within the material. Experiments have shown that these granulated regions significantly increase the detonability of the material through various mechanisms of hot spot formation, and can accelerate the normal combustion rate of the material by several orders of magnitude. Of particular concern is the accidental detonation of solid propellants used in rocket motors which may have been damaged prior to, or during, motor operation (Bernecker and Price 1974a; 1974b). Devices also exist which utilize the energy released by detonation to perform specific tasks within controlled environments. One such device is the Super*Zip separation joint which is regularly used on the Space Shuttle to release spacecraft from the Shuttle's cargo bay. This device, which uses a detonating explosive cord as a mechanism to achieve separation, has malfunctioned during experimental test firings (Bement and Schimmel 1988). The causes of these malfunctions are unclear, but may be attributable to a damaged explosive.

In order to better quantify the risks of accidental detonation in damaged energetic material, or to quantify the effect of material damage on the performance of explosively actuated devices, it is necessary to develop models. To this end, a number of models have been formulated using principles of continuum mixture theory (e.g., Baer and Nunziato 1986; Butler and Krier 1986; Powers et al. 1990a). Though these models have many common features, differences in the functional form of the evolution equations and constitutive models exist. These differences have been the focus of much debate; some relevant issues are discussed in detail by Powers et al. (1990a) and are not repeated here. In addition to the models based on continuum mixture theory, Stewart et al. (1994) formulated a simplified model for predicting detonation in granulated reactive material using a modified single phase state variable approach.

Much of the two-phase detonation modeling effort has focused on predicting the time- dependent events associated with the transition from a low pressure ($\sim 1\ MPa$), low speed ($\sim 100\ m/s$) deflagration wave to a high pressure ($\sim 1\ GPa$), high speed ($\sim 7\ km/s$) detonation wave (Baer and Nunziato 1986; Baer et al. 1986; Butler and Krier 1986; Saurel et al. 1992; Smirnov and Tyurnikov 1994); this process is commonly termed deflagration to detonation transition (DDT). In these studies, the structure of the fully developed detonation waves was not analyzed in detail. However, such an analysis is important because it identifies both existence conditions for

Correspondence to: J.M. Powers

An abridged version of this paper was presented at the 15th Int. Colloquium on the Dynamics of Explosions and Reactive Systems at Boulder, Colorado, from July 30 to August 4, 1995

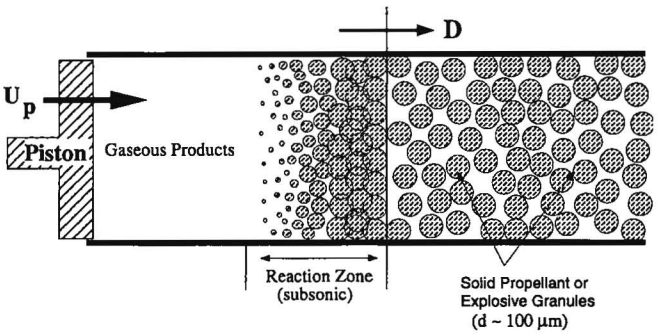

Fig. 1. Schematic of a hypothetical two-phase detonation wave propagating in a granulated material

steady two-phase detonations and the fine length scales occurring within these waves; these fine length scales are often unresolved by coarsely gridded numerical simulations using the unsteady model equations. The fundamental problem of steady detonation structure was studied by Powers et al. (1988; 1990b) in which they classified and discussed steady two-phase detonations within the context of the well-developed theory for one phase detonations (Fickett and Davis 1979). More recently, Embid and Majda (1992) and Embid et al. (1992) have developed an asymptotic theory using the model of Baer and Nunziato (1986) for the transition to detonation in reactive granular materials.

A schematic of a hypothetical two-phase (reactive solid and inert gas) detonation is given in Fig.1; here, the detonation is described within the context of the model formulated by Powers et al. (1990a; 1990b). In this figure, transition to detonation has already occurred due to compression of the material by a piston having a prescribed velocity U_p. The detonation wave, which is propagating to the right with speed D, consists of a single lead shock in the gas and an unshocked solid. Combustion of the solid occurs within the subsonic region of the gas which follows the lead shock; this region is referred to as the reaction zone. At the end of the reaction zone, all of the solid has been completely consumed by combustion. Compression of the gas by the shock, and subsequent heat transfer from the gas to the solid, provides sufficient thermal energy to the solid to initiate combustion. Due to combustion, solid particle mass is converted into gaseous products, with the conversion of chemical energy of the solid into both thermal and kinetic energy of the gas. This energy conversion process sustains the propagation of the wave through the material by means of acoustic energy transmission in the gas from the point of local reaction to the shock.

For piston speeds less than a minimum critical value, $U_{p_{CJ}}$ (which is dependent upon the properties of the explosive, the ambient state of the material, etc.), either a Chapman-Jouguet (CJ) detonation wave or a weak detonation wave may result. Which of these two waves evolves depends upon several factors including the initial bulk density of the material, interphase drag and heat transfer, and material compaction. A steady CJ detonation propagates at a unique speed D_{CJ} such that the velocity of the gas relative to the wave is locally sonic at the end of the reaction zone. A steady weak detonation propagates with speed $D > D_{CJ}$, and the velocity of the gas relative to the wave is locally supersonic at the end of the reaction zone. Both of these waves are self-supported since acoustic waves generated by the moving piston cannot propagate into the reaction zone to influence the detonation. However, for piston speeds in excess of $U_{p_{CJ}}$, the velocity of the gas relative to the wave is such that the flow is subsonic at the end of the reaction zone; consequently, acoustic waves generated by the moving piston do influence the detonation resulting in a piston-supported, or overdriven, wave.

The goal of this study is to numerically predict the time-dependent development of a fully resolved CJ detonation in a granulated material due to compression of the material by a moving piston. The acceleration of the piston is specified as a function of time such that it attains a maximum constant velocity after a time interval which is short relative to the time required for the detonation to develop. The model used in this study was formulated by Powers et al. (1990a). Here, we follow the rationale of that study and adopt certain modeling choices in order to 1) maintain tractability and to 2) allow for direct comparisons of numerical predictions with those given by the steady analysis of Powers et al. (1990b). It is not the emphasis of this study to accurately reproduce all experimentally observed features characteristic of SDT (i.e., transition time, transition length, etc.); rather, the emphasis is on demonstrating the existence of a SDT event which gives rise to a detonation structure predicted by the steady analysis. Nevertheless, the model does predict results commensurate with experiments for the CJ wave speed ($\sim 7500\ m/s$) and the peak detonation pressure ($\sim 20\ GPa$) in granulated HMX. To the best of our knowledge, this work is the first to give detailed comparisons of an unsteady prediction for two-phase detonation structure with the prediction given by a steady-state theory.

The unsteady model equations, which constitute a non-strictly hyperbolic system, are numerically solved using a modern high-resolution method. The numerical method is based on Godunov's method, and utilizes an approximate solution for the two-phase Riemann problem. The utility of this numerical method is in its ability to accurately resolve complicated flow structure involving discontinuities without the explicit addition of artificial viscosity. The numerical method is nominally second order accurate in time and space in regions of smooth flow, but reduces to first order accuracy in space near discontinuities. In addition to the SDT simulation, an inert two-phase shock tube problem is simulated, and the evolution of a compaction wave in response to a moving piston is simulated. For each simulation, the numerically predicted results are compared with known solutions to demonstrate the validity of the numerical method.

Included in this paper are 1) a discussion of the model including both the model assumptions and the equations, 2) a mathematical analysis of the model equations, 3) a discussion of the numerical method, 4) results for the inert two-phase shock tube simulation, the compaction wave simulation, and the SDT simulation, and 5) some conclusions.

2 Model equations

The continuum model used in this study assumes 1) the existence of reactive, spherical solid particles and an inert gas, both having fixed composition, 2) that both phases are fully compressible, 3) that all intraphase diffusive transport processes are negligible, 4) that body forces are negligible, 5) that each phase is in complete non-equilibrium with the other (consequently, each phase can exchange mass, momentum, and energy with the other), and 6) that the two-phase flow is one-dimensional (in a macroscopic sense). The model equations are given in divergence form by the following:

$$\frac{\partial}{\partial t}[\rho_1\phi_1] + \frac{\partial}{\partial x}[\rho_1\phi_1 u_1] = \left(\frac{3}{r}\right)\rho_2\phi_2 a P_1^m, \tag{1}$$

$$\frac{\partial}{\partial t}[\rho_1\phi_1 u_1] + \frac{\partial}{\partial x}\left[\rho_1\phi_1 u_1^2 + P_1\phi_1\right] = u_2\left(\frac{3}{r}\right)\rho_2\phi_2 a P_1^m + \beta\frac{\phi_1\phi_2}{r}(u_2 - u_1), \tag{2}$$

$$\frac{\partial}{\partial t}\left[\rho_1\phi_1\left(e_1 + \frac{u_1^2}{2}\right)\right] + \frac{\partial}{\partial x}\left[\rho_1\phi_1 u_1\left(e_1 + \frac{u_1^2}{2} + \frac{P_1}{\rho_1}\right)\right] = \left(e_2 + \frac{u_2^2}{2}\right)\left(\frac{3}{r}\right)\rho_2\phi_2 a P_1^m + \beta\frac{\phi_1\phi_2}{r}u_2(u_2 - u_1) + h\frac{\phi_1\phi_2}{r^{1/3}}(T_2 - T_1), \tag{3}$$

$$\frac{\partial}{\partial t}[\rho_2\phi_2] + \frac{\partial}{\partial x}[\rho_2\phi_2 u_2] = -\left(\frac{3}{r}\right)\rho_2\phi_2 a P_1^m, \tag{4}$$

$$\frac{\partial}{\partial t}[\rho_2\phi_2 u_2] + \frac{\partial}{\partial x}\left[\rho_2\phi_2 u_2^2 + P_2\phi_2\right] = -u_2\left(\frac{3}{r}\right)\rho_2\phi_2 a P_1^m - \beta\frac{\phi_1\phi_2}{r}(u_2 - u_1), \tag{5}$$

$$\frac{\partial}{\partial t}\left[\rho_2\phi_2\left(e_2 + \frac{u_2^2}{2}\right)\right] + \frac{\partial}{\partial x}\left[\rho_2\phi_2 u_2\left(e_2 + \frac{u_2^2}{2} + \frac{P_2}{\rho_2}\right)\right] = -\left(e_2 + \frac{u_2^2}{2}\right)\left(\frac{3}{r}\right)\rho_2\phi_2 a P_1^m - \beta\frac{\phi_1\phi_2}{r}u_2(u_2 - u_1) - h\frac{\phi_1\phi_2}{r^{1/3}}(T_2 - T_1), \tag{6}$$

$$\frac{\partial}{\partial t}[\rho_2\phi_2^2] + \frac{\partial}{\partial x}[\rho_2 u_2\phi_2^2] = -2\left(\frac{3}{r}\right)\rho_2\phi_2^2 a P_1^m + \frac{\rho_2\phi_1\phi_2^2}{\mu_c}[P_2 - P_1 - f(\phi_2)], \tag{7}$$

$$\frac{\partial n}{\partial t} + \frac{\partial}{\partial x}[u_2 n] = 0, \tag{8}$$

$$P_1 = P_1(\rho_1, e_1), \tag{9}$$

$$e_1 = e_1(\rho_1, T_1), \tag{10}$$

$$c_1^2 = \left.\frac{\partial P_1}{\partial\rho_1}\right|_{s_1} = \frac{P_1}{\rho_1^2}\left.\frac{\partial P_1}{\partial e_1}\right|_{\rho_1} + \left.\frac{\partial P_1}{\partial\rho_1}\right|_{e_1}, \tag{11}$$

$$P_2 = P_2(\rho_2, e_2), \tag{12}$$

$$e_2 = e_2(\rho_2, T_2), \tag{13}$$

$$c_2^2 = \left.\frac{\partial P_2}{\partial\rho_2}\right|_{s_2} = \frac{P_2}{\rho_2^2}\left.\frac{\partial P_2}{\partial e_2}\right|_{\rho_1} + \left.\frac{\partial P_2}{\partial\rho_2}\right|_{e_2}, \tag{14}$$

$$n = \frac{3\phi_2}{4\pi r^3}, \tag{15}$$

$$\phi_1 + \phi_2 = 1. \tag{16}$$

In these equations, the subscripts "1" and "2" denote quantities associated with the gas and solid, respectively. The independent variables are time t and position x. Dependent variables are as follows: the phase density ρ_i ($i = 1, 2$), defined as the mass of phase i per unit volume occupied by that phase; the phase pressure P_i; the phase temperature T_i; the particle velocity measured with respect to a stationary reference frame u_i; the specific internal energy e_i; the specific entropy s_i; the sound speed c_i; the volume fraction ϕ_i, defined as the ratio of the volume occupied by phase i to the total volume; the radius of the spherical solid particles r; and the number of solid particles per unit volume n.

Equations (1-3) are evolution equations for the mass, momentum, and energy of the gas. Equations (4-6) are evolution equations for the mass, momentum, and energy of the solid. These evolution equations are constructed such that when Eqs. (1) and (4), Eqs. (2) and (5), and Eqs. (3) and (6) are added, respectively, the forcing terms cancel yielding conservation equations for the mixture mass, momentum, and energy. Furthermore, it is easily shown that these equations are frame-invariant under a Galilean transformation.

The forcing terms in Eqs. (1) and (4) account for the exchange of mass from the solid to the gas due to combustion. Here, mass exchange is modeled as a single, irreversible process (*solid→inert gas*), and all chemical reaction is confined to the particle surface. Combustion initiation is assumed to occur when $T_1 \geq T_{ig}$, where T_{ig} is a constant ignition temperature. The combustion rate is modeled by a gas phase pressure-dependent burn law; such an assumption is commonly made in solid propellant combustion modeling. Values for the combustion rate parameters a and m are assumed constant for this study.

The forcing terms in Eqs. (2) and (5) account for two forms of momentum exchange between the gas and solid. First, the gas is gaining that momentum associated with the solid which is being converted into gas due to combustion. Second, there is an exchange of momentum due to solid particle-gas drag interaction. This interaction is modeled by a drag law which states that the drag is proportional to the difference in velocity between the phases and inversely proportional to the particle radius. In the drag law, β is defined as a constant drag coefficient.

The forcing terms in Eqs. (3) and (6) account for the exchange of energy between the gas and solid. Energy exchange associated with combustion, and with particle-gas drag interaction are accounted for, as is the exchange of thermal energy between the gas and solid. The thermal energy exchange rate is assumed to be proportional to the temperature difference between the gas and the solid and inversely proportional to

the cube root of the particle radius. In the expression governing thermal energy exchange, h is defined as a constant heat transfer coefficient.

Equation (7) is a dynamic compaction equation describing changes in solid volume fraction due to both compaction and combustion of the granular material. This equation predicts that, in the absence of combustion, the solid volume fraction, ϕ_2, will equilibrate to a value such that the solid phase pressure, P_2, equals the sum of the gas phase pressure, P_1, and an intragranular, or configurational, stress, f, which is assumed to vary with ϕ_2; the equilibration rate is governed by the constant parameter μ_c which is termed the compaction viscosity.

Equation (8) is an evolution equation for the particle number density. This equation expresses that the total number of particles in the system is conserved.

Equations (9-11) and (12-14) are functional dependencies for the thermal and caloric equations of state, and the definition for the sound speed for the gas and the solid, respectively. Equation (15) is the definition for particle number density expressed in terms of the solid volume fraction and the particle radius, and Eq. (16) is a saturation condition.

3 Mathematical analysis of the model equations

Using vector notation, Eqs. (1-8) can be expressed in the standard divergence form

$$\frac{\partial \mathbf{q}}{\partial t} + \frac{\partial \mathbf{f}(\mathbf{q})}{\partial x} = \mathbf{g}(\mathbf{q}), \tag{17}$$

where

$$\mathbf{q} = \left[\rho_1\phi_1,\ \rho_1\phi_1 u_1,\ \rho_1\phi_1(e_1 + u_1^2/2),\ \rho_2\phi_2,\ \rho_2\phi_2 u_2,\right.$$
$$\left.\rho_2\phi_2(e_2 + u_2^2/2),\ \rho_2\phi_2^2,\ n\right]^T,$$

$$\mathbf{f}(\mathbf{q}) = \left[\rho_1\phi_1 u_1,\ \rho_1\phi_1 u_1^2 + P_1\phi_1,\ \rho_1\phi_1 u_1(e_1 + u_1^2/2 + P_1/\rho_1),\right.$$
$$\rho_2\phi_2 u_2,\ \rho_2\phi_2 u_2^2 + P_2\phi_2,\ \rho_2\phi_2 u_2(e_2 + u_2^2 + P_2/\rho_2),$$
$$\left.\rho_2 u_2\phi_2^2,\ u_2 n\right]^T,$$

$$\mathbf{g}(\mathbf{q}) = \left[(3/r)\rho_2\phi_2 a P_1^m,\ u_2(3/r)\rho_2\phi_2 a P_1^m\right.$$
$$+\beta\phi_1\phi_2(u_2 - u_1)/r,\ (e_2 + u_2^2)(3/r)\rho_2\phi_2 a P_1^m$$
$$+\beta\phi_1\phi_2 u_2(u_2 - u_1)/r\ + h\phi_1\phi_2(T_2 - T_1)/r^{1/3},$$
$$-(3/r)\rho_2\phi_2 a P_1^m,\ -u_2(3/r)\rho_2\phi_2 a P_1^m$$
$$-\beta\phi_1\phi_2(u_2 - u_1)/r,\ -(e_2 + u_2^2)(3/r)\rho_2\phi_2 a P_1^m$$
$$-\beta\phi_1\phi_2 u_2(u_2 - u_1)/r - h\phi_1\phi_2(T_2 - T_1)/r^{1/3},$$
$$\left.-2(3/r)\rho_2\phi_2^2 a P_1^m + \rho_2\phi_1\phi_2^2(P_2 - P_1 - f)/\mu_c,\ 0\right]^T.$$

Equivalently, Eq. (17) can be expressed in the non-divergence form

$$\frac{\partial \mathbf{q}}{\partial t} + \mathbf{A}(\mathbf{q})\frac{\partial \mathbf{q}}{\partial x} = \mathbf{g}(\mathbf{q}), \tag{18}$$

where the flux Jacobian $\mathbf{A}(\mathbf{q}) \equiv \partial \mathbf{f}(\mathbf{q})/\partial \mathbf{q}$ is the 8×8 matrix

$$\begin{bmatrix}
0 & 1 & 0 \\
c_1^2 - u_1^2 - \left(H_1 - u_1^2\right)\Gamma_1 & 2u_1 - u_1\Gamma_1 & \Gamma_1 \\
u_1\left(c_1^2 - H_1\right) - u_1\left(H_1 - u_1^2\right)\Gamma_1 & H_1 - u_1^2\Gamma_1 & u_1 + u_1\Gamma_1 \\
0 & 0 & 0 \\
0 & 0 & 0 \\
0 & 0 & 0 \\
0 & 0 & 0 \\
0 & 0 & 0
\end{bmatrix}$$

$$\begin{bmatrix}
0 & 0 \\
-\rho_1\eta_1/\rho_2 & 0 \\
-u_1\rho_1\eta_1/\rho_2 & 0 \\
0 & 1 \\
c_2^2 - u_2^2 - \left(H_2 - u_2^2\right)\Gamma_2 + \eta_2 & 2u_2 - u_2\Gamma_2 \\
u_2\left(c_2^2 - H_2\right) - u_2\left(H_2 - u_2^2\right)\Gamma_2 + u_2\eta_2 & H_2 - u_2^2\Gamma_2 \\
-\phi_2 u_2 & \phi_2 \\
-u_2 n/(\rho_2\phi_2) & n/(\rho_2\phi_2)
\end{bmatrix}$$

$$\begin{bmatrix}
0 & 0 & 0 \\
0 & \rho_1\eta_1/(\rho_2\phi_2) & 0 \\
0 & u_1\rho_1\eta_1/(\rho_2\phi_2) & 0 \\
0 & 0 & 0 \\
\Gamma_2 & -\eta_2/\phi_2 & 0 \\
u_2 + u_2\Gamma_2 & -u_2\eta_2/\phi_2 & 0 \\
0 & u_2 & 0 \\
0 & 0 & u_2
\end{bmatrix} \tag{19}$$

Here, the total enthalpies H_1 and H_2 are defined by

$$H_1 \equiv e_1 + \frac{u_1^2}{2} + \frac{P_1}{\rho_1}, \qquad H_2 \equiv e_2 + \frac{u_2^2}{2} + \frac{P_2}{\rho_2}, \tag{20}$$

and the Grüneisen coefficients Γ_1 and Γ_2 are defined by

$$\Gamma_1 \equiv \frac{1}{\rho_1}\left.\frac{\partial P_1}{\partial e_1}\right|_{\rho_1}, \qquad \Gamma_2 \equiv \frac{1}{\rho_2}\left.\frac{\partial P_2}{\partial e_2}\right|_{\rho_2}. \tag{21}$$

Additionally, the following variables have been introduced into Eq. (19) for compactness:

$$\eta_1 \equiv c_1^2 - (\Gamma_1 + 1)\frac{P_1}{\rho_1}, \qquad \eta_2 \equiv c_2^2 - (\Gamma_2 + 1)\frac{P_2}{\rho_2}. \tag{22}$$

It is noted that for calorically perfect ideal equations of state for the gas and solid, $\eta_i \equiv 0$ $(i = 1, 2)$.

The mathematical classification of the model equations requires an analysis of the eigenvalues $\lambda^{(k)}$ $(k = 1, \ldots, 8)$ and corresponding right eigenvectors $\mathbf{r}^{(k)}$ $(k = 1, \ldots, 8)$ of $\mathbf{A}(\mathbf{q})$. The $\lambda^{(k)}$ and $\mathbf{r}^{(k)}$ are given by

$$\lambda^{(1)} = u_1, \quad \lambda^{(2)} = u_1 + c_1, \quad \lambda^{(3)} = u_1 - c_1, \quad \lambda^{(4)} = u_2,$$
$$\lambda^{(5)} = u_2 + c_2, \quad \lambda^{(6)} = u_2 - c_2, \quad \lambda^{(7)} = u_2, \quad \lambda^{(8)} = u_2, \tag{23}$$

$$\mathbf{r}^{(1)} = \left[1,\ u_1,\ H_1 - c_1^2/\Gamma_1,\ 0,\ 0,\ 0,\ 0,\ 0\right]^T, \tag{24}$$

$$\mathbf{r}^{(2)} = \left[1,\ u_1 + c_1,\ H_1 + u_1 c_1,\ 0,\ 0,\ 0,\ 0,\ 0\right]^T, \tag{25}$$

$$\mathbf{r}^{(3)} = \left[1,\ u_1 - c_1,\ H_1 - u_1 c_1,\ 0,\ 0,\ 0,\ 0,\ 0\right]^T, \tag{26}$$

$$\mathbf{r}^{(4)} = \left[0,\ 0,\ 0,\ 1,\ u_2,\ H_2 - c_2^2/\Gamma_2,\ \phi_2,\ 0\right]^T, \tag{27}$$

$$\mathbf{r}^{(5)} = [0,\ 0,\ 0,\ 1,\ u_2 + c_2,\ H_2 + u_2 c_2,\ \phi_2,\ n/(\rho_2\phi_2)]^T, \tag{28}$$

$$\mathbf{r}^{(6)} = [0,\ 0,\ 0,\ 1,\ u_2 - c_2,\ H_2 - u_2 c_2,\ \phi_2,\ n/(\rho_2\phi_2)]^T, \tag{29}$$

$$\mathbf{r}^{(7)} = \left[\frac{\rho_1\eta_1}{\rho_2\phi_2\left((u_2-u_1)^2 - c_1^2\right)},\ \frac{\rho_1\eta_1 u_2}{\rho_2\phi_2\left((u_2-u_1)^2 - c_1^2\right)},\ \frac{\rho_1\eta_1\left(H_1 + u_1u_2 - u_1^2\right)}{\rho_2\phi_2\left((u_2-u_1)^2 - c_1^2\right)}, 0,\ 0,\ \frac{\eta_2}{\phi_2\Gamma_2},\ 1,\ 0\right]^T, \tag{30}$$

$$\mathbf{r}^{(8)} = [0,\ 0,\ 0,\ 0,\ 0,\ 0,\ 0,\ 1]^T. \tag{31}$$

Here, $\lambda^{(1)}$ and $\mathbf{r}^{(1)}$, $\lambda^{(2)}$ and $\mathbf{r}^{(2)}$, and $\lambda^{(3)}$ and $\mathbf{r}^{(3)}$ are associated with the propagation of entropy waves, forward traveling acoustic waves, and backward traveling acoustic waves in the gas, respectively; $\lambda^{(4)}$ and $\mathbf{r}^{(4)}$, $\lambda^{(5)}$ and $\mathbf{r}^{(5)}$, and $\lambda^{(6)}$ and $\mathbf{r}^{(6)}$ are associated with the propagation of entropy waves, forward traveling acoustic waves, and backward traveling acoustic waves in the solid, respectively; $\lambda^{(7)}$ and $\mathbf{r}^{(7)}$ are associated with the propagation of infinitesimal disturbances in volume fraction; and, $\lambda^{(8)}$ and $\mathbf{r}^{(8)}$ are associated with the propagation of infinitesimal disturbances in particle number density.

Following Zauderer (1989), a system of equations having the form of Eq. (18) is classified as strictly hyperbolic if for each x, t, and $\mathbf{q}$, the eigenvalues of $\mathbf{A}(\mathbf{q})$ are real and distinct; in such a case, a linearly independent set of right eigenvectors exists. If the eigenvalues are real but not distinct, then the system of equations is non-strictly hyperbolic provided that the corresponding right eigenvectors are linearly independent. In the event that the eigenvalues are real but not distinct, and the right eigenvectors are not linearly independent, then the system of equations is parabolic.

Since the eigenvalues given by Eq. (23) are real but not distinct, the model equations constitute a non-strictly hyperbolic system provided that the right eigenvectors [Eqs. (24-31)] are linearly independent. Linear independence requires that the matrix of right eigenvectors $\mathbf{R} \equiv [\mathbf{r}^{(1)}|\mathbf{r}^{(2)}|\cdots|\mathbf{r}^{(8)}]$ be non-singular. It is shown by Gonthier (1996) that the right eigenvectors are linearly independent except at the singular points $\phi_2 = 0$ and $u_2 = u_1 \pm c_1$. For $\phi_2 = 0$, the forward and backward acoustic eigenvectors for the solid, $\mathbf{r}^{(5)}$ and $\mathbf{r}^{(6)}$ respectively, degenerate (upon proper scaling) into the particle number density eigenvector $\mathbf{r}^{(8)}$:

$$\lim_{\phi_2\to 0}\left[\frac{\rho_2\phi_2}{n}\mathbf{r}^{(5)}\right] = \lim_{\phi_2\to 0}\left[\frac{\rho_2\phi_2}{n}\mathbf{r}^{(6)}\right] = \mathbf{r}^{(8)}.$$

For $u_2 = u_1 + c_1$ and $u_2 = u_1 - c_1$, the compaction eigenvector $\mathbf{r}^{(7)}$ degenerates (upon proper scaling) into the gas phase forward and backward acoustic eigenvectors $\mathbf{r}^{(2)}$ and $\mathbf{r}^{(3)}$, respectively:

$$\lim_{u_2\to u_1+c_1}\left[\frac{\rho_2\phi_2\left((u_2-u_1)^2 - c_1^2\right)}{\rho_1\eta_1}\mathbf{r}^{(7)}\right] = \mathbf{r}^{(2)},$$

$$\lim_{u_2\to u_1-c_1}\left[\frac{\rho_2\phi_2\left((u_2-u_1)^2 - c_1^2\right)}{\rho_1\eta_1}\mathbf{r}^{(7)}\right] = \mathbf{r}^{(3)}.$$

Consequently, the model equations constitute a non-strictly hyperbolic system having parabolic degeneracies on the manifolds $\phi_2 = 0$ and $u_2 = u_1 \pm c_1$ in phase space. Similar singularities have been identified in the two-phase model proposed by Baer and Nunziato (1986); a detailed discussion is given by Embid and Baer (1992).

4 Numerical method

Since the model equations are hyperbolic, discontinuous solutions are admitted (Whitham 1974). As such, a requirement of any numerical method used to solve these equations is the ability to accurately resolve discontinuities. Several high-resolution methods have been developed for this purpose for strictly hyperbolic systems such as the Euler equations of gas dynamics (e.g., Roe 1981; Osher and Solomon 1982; Osher 1984). Many of these methods are based on Godunov's method which requires the exact or approximate solution of a Riemann problem at computational cell interfaces in order to advance the solution in time. The numerical method described herein was formulated using concepts associated with these well-developed methods for strictly hyperbolic systems. A summary of the numerical method is given below; details of the method are given by Gonthier (1996).

The spatial domain $x \in [x_{min}, x_{max}]$ is discretized into N uniformly spaced nodes located at the points $x_j = x_{min} + (j-1)\Delta x$ $(j = 1, \ldots, N)$, where $\Delta x = (x_{max} - x_{min})/(N-1)$. Each node x_j $(j = 2, \ldots, N-1)$ is located at the center of a computational cell of width Δx; the location of the cell boundaries are denoted as $x_{j\pm 1/2}$. The nodes x_1 and x_N are located at the boundaries of the computational domain.

The model equations are numerically solved on the computational grid using the method of fractional steps (Strang 1968):

$$\mathbf{Q}^{n+2} = \mathscr{L}_c^{\Delta t}\mathscr{L}_s^{\Delta t}\mathscr{L}_s^{\Delta t}\mathscr{L}_c^{\Delta t}\mathbf{Q}^n, \tag{32}$$

where $\mathbf{Q}^{n+2}$ and $\mathbf{Q}^n$ are numerical approximations for $\mathbf{q}$ at times $t = (n+2)\Delta t$ and $t = n\Delta t$, respectively. The numerical operator $\mathscr{L}_c^{\Delta t}$ represents the method used to solve the homogeneous model equations [obtained by setting $\mathbf{g}(\mathbf{q}) = 0$ in Eq. (17)] which account for nonlinear convection. The numerical operator $\mathscr{L}_s^{\Delta t}$ represents the method used to solve the coupled system of ordinary differential equations (ODEs) [obtained by setting $\partial/\partial x = 0$ in Eq. (17)] which account for the phase interaction processes. Here, the splitting procedure requires that each successive numerical step be performed over a time interval Δt which is chosen based upon a local Courant-Friedrichs-Lewy (CFL) condition $\Delta t = (\mathrm{CFL})\Delta x/|\lambda|_{max}$, where CFL is a dimensionless number. All simulations performed in this study used CFL = 0.4.

The numerical method used in the convective step is based on Godunov's method. Since the Riemann problem for this two-phase system has not been analytically studied, an approximate solution is used in the numerical method (see Appendix

A). The approximate Riemann solution is obtained by an approach similar to that used by Glaister (1988) to formulate an approximate Riemann solution for the Euler equations for a non-ideal gas. Implicit in the construction of the approximate solution for the two- phase Riemann problem is the assumption that a physically relevant exact solution exists which consists of at most eight waves: a 1) shock wave, 2) rarefaction wave, and 3) contact discontinuity (entropy wave) in the gas; a 4) shock wave, 5) rarefaction wave, and 6) contact discontinuity in the solid; a 7) compaction wave; and a 8) particle number density wave. The convective step $\mathscr{L}_c^{\Delta t}\mathbf{Q}^n$, which uses a predictor/corrector Runge-Kutta integration procedure for increased temporal accuracy, is as follows:

$$\overline{\mathbf{Q}}_j = \mathbf{Q}_j^n - \frac{\Delta t}{2\Delta x}\left(\mathbf{F}_{j+1/2}^{(H)} - \mathbf{F}_{j-1/2}^{(H)}\right), \tag{33}$$

$$\mathbf{Q}_j^{n+1} = \mathbf{Q}_j^n - \frac{\Delta t}{\Delta x}\left(\overline{\mathbf{F}}_{j+1/2}^{(H)} - \overline{\mathbf{F}}_{j-1/2}^{(H)}\right), \tag{34}$$

where

$$\mathbf{F}_{j+1/2}^{(H)} = \mathbf{F}_{j+1/2}^{(L)} + \mathbf{F}_{j+1/2}^{(C)}.$$

Here, $\mathbf{F}_{j+1/2}^{(H)}$ and $\overline{\mathbf{F}}_{j+1/2}^{(H)}$ are higher order numerical fluxes evaluated using the initial data $\mathbf{Q}^n$ and the intermediate data $\overline{\mathbf{Q}}$, respectively. The higher order numerical flux consists of a lower order numerical flux $\mathbf{F}_{j+1/2}^{(L)}$ and a corrective flux $\mathbf{F}_{j+1/2}^{(C)}$. The lower order flux, which introduces significant numerical diffusion into the method, is determined from the approximate solution of the Riemann problem. The corrective flux is constructed using flux extrapolation and is limited based upon the local solution behavior in order to achieve nominally second order spatial accuracy in smooth regions of the flow (Chakravarthy and Osher 1985). Near discontinuities, the corrective flux is suppressed allowing the numerical diffusion inherent in the lower order flux to prevent the generation of spurious oscillations.

The numerical method used in the source step is a stiff ODE solver contained in the standard package LSODE. To obtain $\mathbf{Q}^{n+1}$, given the initial data $\mathbf{Q}^n$, the source step $\mathscr{L}_s^{\Delta t}\mathbf{Q}^n$ requires the solution of a system of ODEs having the following form at each computational node x_j ($j = 1, \ldots, N$):

$$\frac{d}{dt}\begin{bmatrix}\rho_2\\ u_2\\ e_2\\ \phi_2\end{bmatrix} = \begin{bmatrix}h_1(\rho_2, u_2, e_2, \phi_2)\\ h_2(\rho_2, u_2, e_2, \phi_2)\\ h_3(\rho_2, u_2, e_2, \phi_2)\\ h_4(\rho_2, u_2, e_2, \phi_2)\end{bmatrix}. \tag{35}$$

Here, h_1, h_2, h_3, and h_4 are nonlinear algebraic functions of the solid phase variables. Equation (35) is obtained by reducing the system of ODEs given by Eq. (17) with $\partial/\partial x = 0$. The reductions involve obtaining algebraic expressions for ρ_1, u_1, e_1, ϕ_1, and n in terms of the solid phase variables and the initial data $\mathbf{Q}^n$.

Difficulties are encountered in the numerical method near the singularities $u_2 = u_1 \pm c_1$ and $\phi_2 = 0$. At these points, the model equations become parabolic and the numerical method breaks down. Bell et al. (1989) describe modifications to the Godunov methodology which are needed to suppress numerical instabilities resulting from a loss of hyperbolicity. To avoid difficulties near the singularities $u_2 = u_1 \pm c_1$, a technique similar to that given by Bell et al. is adopted. To avoid difficulties near the singularity $\phi_2 = 0$, combustion is terminated when the local solid volume fraction is less than 1.0×10^{-4}; thus, the solid particles are assumed to have an inert solid core. It is noted that this complete combustion singularity also exists in the steady-state model and, within the context of that model, has been shown to be inconsequential (Powers et al. 1990b).

5 Results

Results are presented for three different simulations: 1) an inert two-phase shock tube problem, 2) the evolution of a compaction wave in response to a moving piston, and 3) the evolution of a detonation wave in response to a moving piston. Comparisons are made with exact solutions for the shock tube problem, with predictions given by a simplified steady state theory for the compaction wave structure, and with predictions given by a formal steady state theory for the detonation wave structure. The computations were performed on an IBM RS6000 Model 350 workstation.

5.1 Two-phase shock tube simulation

The two-phase shock tube problem involves the breakup of a single initial discontinuity separating constant left (L) and right (R) states into self-similar waves consisting of a shock wave, a rarefaction wave, and a contact discontinuity in both the gas and the solid. This problem considers convection only; consequently, $\mathbf{g}(\mathbf{q}) = 0$ in Eq. (17). In this simulation, an ideal equation of state was used for the gas [$P_1 = \rho_1 R_1 T_1$; $e_1 = c_{v1} T_1$] and a constant covolume non-ideal equation of state was used for the solid [$P_2 = \rho_2 R_2 T_2/(1 - b\rho_2)$; $e_2 = c_{v2} T_2$] (Toro 1989). These state equations were chosen solely to compare numerical predictions with existing closed-form analytical solutions. Values chosen for the model parameters and the initial conditions are given in Table 1. The initial discontinuity was located at the position $x = 0\ m$. For this simulation, 200 computational nodes were used.

Shown in Figs. 2a-c is a comparison between the numerical and exact solution at time $t = 5\ ms$. In these figures, all quantities have been scaled by the corresponding maximum exact values. For each phase, the solution consists of a right propagating shock wave, followed by a slower moving right propagating contact discontinuity, and a left propagating rarefaction wave. Also, a jump is predicted in the particle number density (n) across both the shock and the contact discontinuity in the solid; a continuous variation in n is predicted across the rarefaction wave. Good agreement exists between the numerically predicted solution and the exact solution.

A convergence study was performed for this solution using computational grids ranging from 100 to 15000 nodes. Results of this study showed the rate of convergence to be $\Delta x^{1.003}$. Machine round-off error was insignificant for this range of nodal points.

Table 1. Parameters and initial conditions (IC's) used in the two-phase shock tube simulation

Parameter or IC	Value	Units
b	5.00×10^{-2}	m^3/kg
c_{v1}	7.18×10^2	$J/kg/K$
c_{v2}	7.18×10^2	$J/kg/K$
R_1	2.87×10^2	$J/kg/K$
R_2	2.87×10^2	$J/kg/K$
u_{1L}	0	m/s
u_{2L}	0	m/s
u_{1R}	0	m/s
u_{2R}	0	m/s
ρ_{1L}/ρ_{1R}	1.00×10^1	
ρ_{2L}/ρ_{2R}	1.00×10^1	
P_{1L}/P_{1R}	1.00×10^1	
P_{2L}/P_{2R}	1.00×10^1	
n_L/n_R	1.00×10^0	

5.2 Compaction wave simulation

This simulation considers the evolution of an inert compaction wave due to compression of the material by an accelerating piston. The piston accelerates from rest at $t = 0\ \mu s$ to a constant velocity of 100 m/s at $t = 2.0\ \mu s$. Here, a compaction wave refers to the propagation of a finite disturbance in the porosity of the system due to mechanical stresses. In this simulation, a virial equation of state was used for the gas [$P_1 = \rho_1 R_1 T_1(1 + b\rho_1)$; $e_1 = c_{v1} T_1$], and a non-ideal Tait equation of state was used for the solid [$P_2 = (\gamma_2 - 1)c_{v2}\rho_2 T_2 - \rho_{2o}\sigma/\gamma_2$; $e_2 = c_{v2}T_2 + \rho_{2o}\sigma/\gamma_2\rho_2 + q$]; also, the configurational stress $f(\phi_2)$ given by Powers et al. (1989) was used:

$$f = (P_{2o} - P_{1o})\frac{\phi_2^2}{\phi_{2o}^2}\frac{(2-\phi_{2o})^2}{(2-\phi_2)^2}\frac{\ln(\frac{1}{1-\phi_2})}{\ln(\frac{1}{1-\phi_{2o}})}. \tag{36}$$

In this expression, quantities labeled with subscript "o" are associated with the ambient state of the material. For this simulation, the model equations were transformed to a reference frame moving with the piston such that the transformed velocities at the piston surface were zero. Reflective boundary conditions were enforced at the piston surface. No boundary conditions were enforced at the upstream boundary since time was restricted such that there was insufficient time for the wave to reach this boundary. The computational domain, which consisted of 600 nodes, was initialized with the ambient state given in Table 2. Values for the model parameters are also given in Table 2. The computational run time for this simulation was approximately 45 minutes.

Figures 3a,b show the gas and solid pressure histories. In these figures, ξ is the position measured in the piston-attached coordinate system (the piston surface is located at $\xi = 0\ m$). A smooth increase is initially predicted in both the gas and solid pressure in response to the moving piston. The gas pressure rises from its ambient value of 2.58 MPa to a maximum value of 28.26 MPa in 0.3 ms; the solid pressure rises from its ambient value of 9.12 MPa to a maximum value of 69.16 MPa in 0.2 ms. Subsequently, both pressures remain essentially constant as a steady compaction wave develops and propagates away from the piston. Though not shown here, there is also a smooth increase in the other state variables across the compaction wave. The predicted length and time for transition to a fully developed compaction wave are approximately 0.1 m (measured relative to the piston) and 0.6 ms, respectively. The

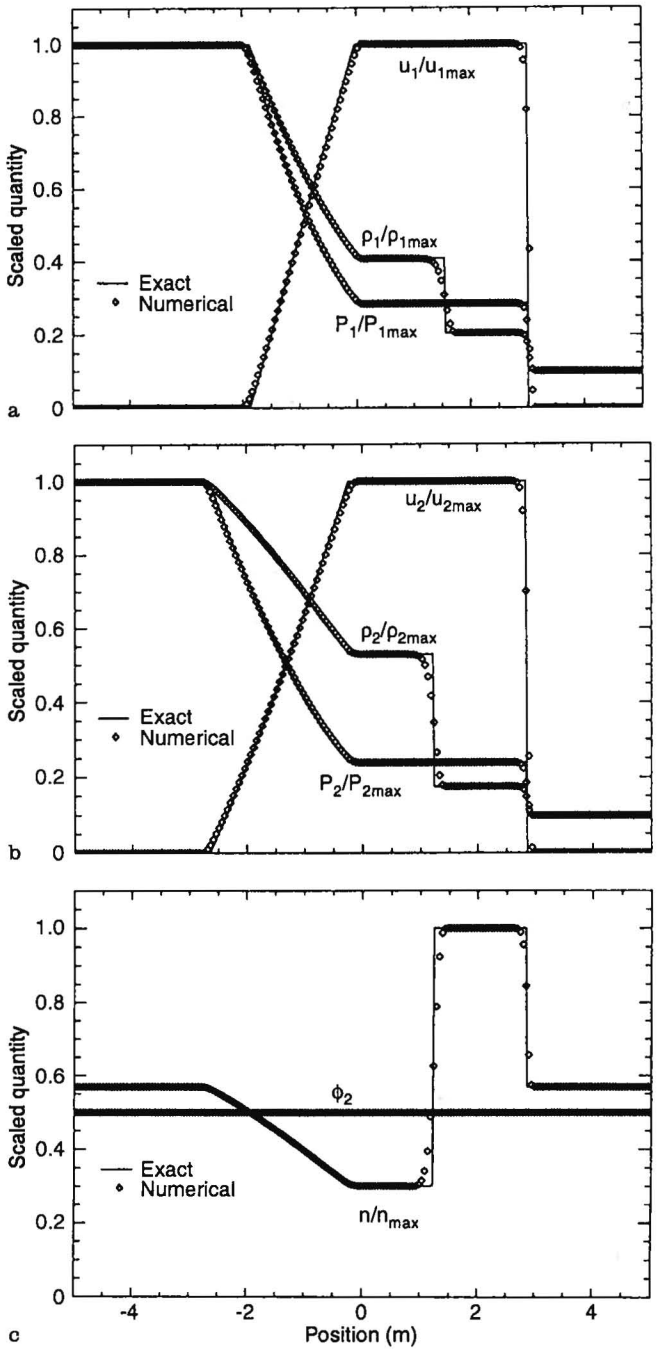

Fig. 2a–c. Comparison of the numerical and exact solution for the two-phase shock tube simulation at $t = 5\ ms$: **a** gas phase quantities, **b** solid phase quantities, and **c** solid volume fraction and particle number density

Table 2. Parameters and initial conditions (IC's) used in the compaction wave and the detonation wave simulations

Parameter or IC	Compaction (Numerical 1)	Compaction (Numerical 2)	Detonation	Units
b	1.10×10^{-3}	1.10×10^{-3}	1.10×10^{-3}	m^3/kg
R_1	8.50×10^{2}	8.50×10^{2}	8.50×10^{2}	$J/kg/K$
c_{v1}	2.40×10^{3}	2.40×10^{3}	2.40×10^{3}	$J/kg/K$
c_{v2}	1.50×10^{3}	1.50×10^{3}	1.50×10^{3}	$J/kg/K$
γ_2	5.00×10^{0}	5.00×10^{0}	5.00×10^{0}	
σ	8.98×10^{6}	8.98×10^{6}	8.98×10^{6}	$(m/s)^2$
q	0	0	5.84×10^{6}	J/kg
a	0	0	2.90×10^{-9}	$m/(sPa)$
m			1.00×10^{0}	
β	0	1.00×10^{4}	1.00×10^{4}	$kg/s/m^2$
h	0	1.00×10^{7}	1.00×10^{7}	$J/(sKm^{8/3})$
μ_c	1.00×10^{3}	1.00×10^{3}	1.00×10^{6}	$kg/m/s$
T_{ig}			3.10×10^{2}	K
r_o	1.00×10^{-4}	1.00×10^{-4}	1.00×10^{-4}	m
ϕ_{2o}	7.30×10^{-1}	7.30×10^{-1}	7.30×10^{-1}	
T_o	3.00×10^{2}	3.00×10^{2}	3.00×10^{2}	K
ρ_{1o}	1.00×10^{1}	1.00×10^{1}	1.00×10^{1}	kg/m^3
ρ_{2o}	1.90×10^{3}	1.90×10^{3}	1.90×10^{3}	kg/m^3

thickness of the resulting compaction wave is predicted to be approximately 8 cm.

Figures 4a,b show the numerically predicted variation in solid pressure and volume fraction within the compaction wave. Also shown in these figures is the steady wave structure predicted by the simplified analysis of Powers et al. (1989). In their analysis, Powers et al. ignore gas phase effects and describe steady compaction wave structure in terms of the solid variables. In these figures, the flow located between the piston ($\xi = 0$) and the trailing edge of the compaction wave ($\xi = 0.55$ m) is not shown. The prediction labeled Numerical 1 did not account for interphase drag and heat transfer so that a direct comparison between the numerical and theoretical predictions for compaction wave structure could be made. The prediction labeled Numerical 2 is for the simulation shown in Figs. 4a,b at $t = 2$ ms. As seen in these figures, the numerical and theoretical predictions agree well. It is noted that a dispersed compaction wave structure is predicted, and that the inclusion of interphase drag and heat transfer increases the final solid pressuré and decreases the final solid volume fraction. The wave speed predicted by the steady analysis of Powers et al. is 404 m/s which agrees well with the numerically predicted value of 407 m/s for the simulation denoted as Numerical 1. The wave speed predicted for the simulation denoted as Numerical 2 is 430 m/s. Experimentally observed compaction wave speeds of 432 m/s in porous HMX ($\phi_{2o} = 0.73$) resulting from the impact of a 100 m/s piston have been reported by Sandusky and Liddiard (1985).

A convergence study was performed for the solution denoted as Numerical 1 using computational grids ranging from 300 to 5000 nodes. The results of this study showed the rate of convergence to be $\Delta\xi^{1.541}$.

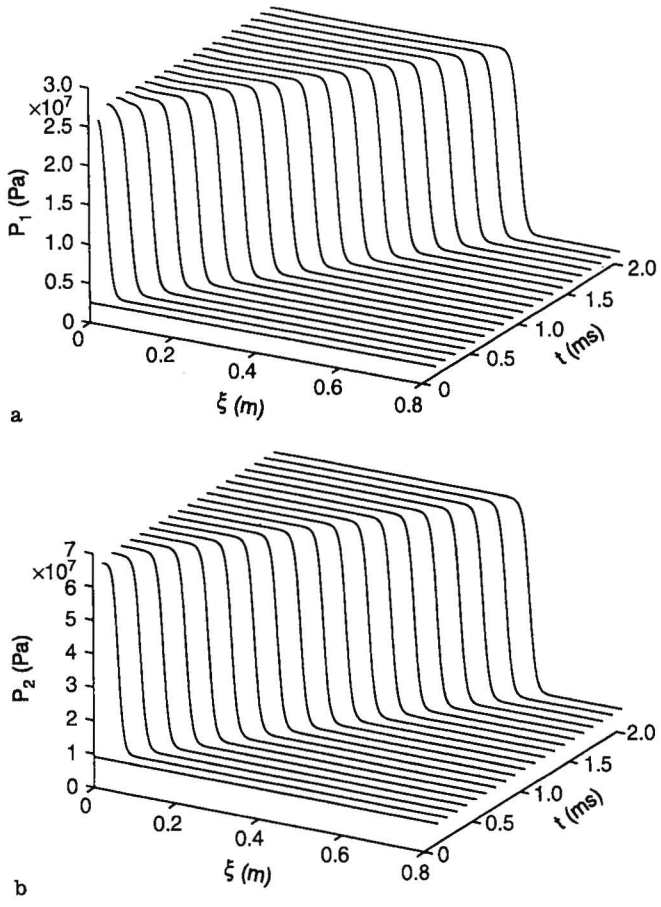

Fig. 3a,b. a Gas and **b** solid pressure history for the compaction wave simulation

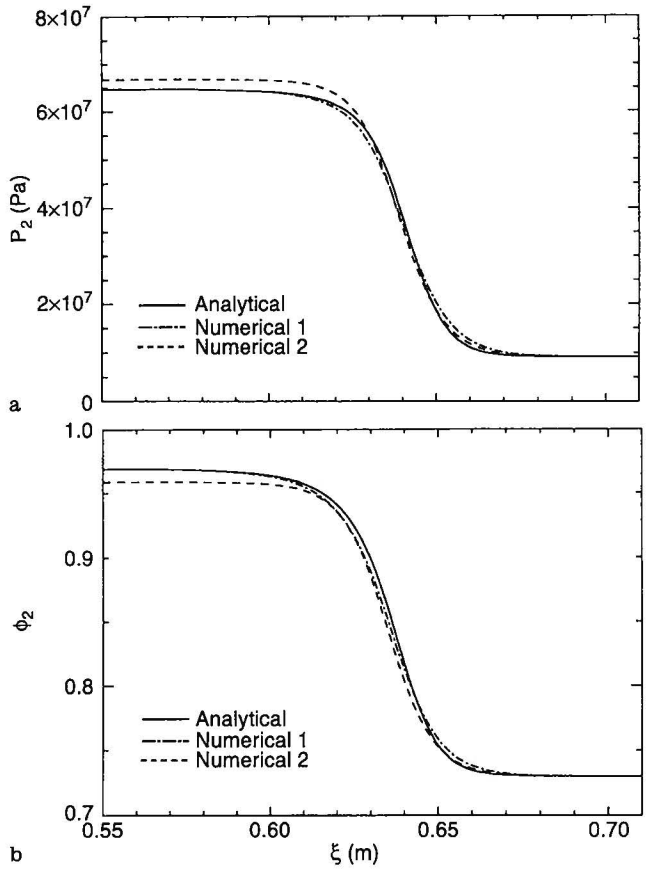

Fig. 4a,b. Comparison of numerical predictions with the analytical prediction given by Powers et al. (1989) for the compaction wave structure: **a** solid pressure, and **b** solid volume fraction. (The prediction labeled Numerical 1 does not account for interphase drag and heat transfer.)

5.3 Detonation wave simulation

This simulation considers the evolution of a two-phase detonation wave due to compression of the material by a moving piston. The results presented here were obtained for a piston having the same prescribed motion as for the compaction wave simulation presented in the previous subsection. The same state equations, boundary conditions, and initial conditions used in the compaction wave simulation were also used here; however, the following configurational stress $f(\phi_2)$ given by Powers et al. (1990b) was used so that proper comparisons could be made with the published results of that study:

$$f = \frac{P_{2o} - P_{1o}}{\phi_{2o}} \phi_2 .$$

Numerical simulations have shown that this relation predicts compaction wave speeds which are substantially higher than those observed in experiments; as such, the experiments would be better modeled using the configurational stress given by Eq. (36). Values for the model parameters are given in Table 2. For this simulation, the computational domain consisted of 1000 nodes and the computational run time was approximately 2 hours.

Figures 5a-d show the velocity and pressure histories for the gas and solid, respectively. In these figures, the curves for the solid phase quantities are plotted up to the point of complete combustion (i.e., for $\phi_2 \geq 1.0 \times 10^{-4}$). Initially, a dispersed compaction wave is predicted to propagate away from the piston with a speed of 2600 m/s. Onset of combustion occurs near the piston surface when the gas temperature exceeds $T_{ig} = 310\ K$, the value of which was chosen ad hoc. The combustion rate then accelerates due to the increasing gas pressure, strengthens, and undergoes transition to detonation near $\xi = 0.06\ m$ at $t = 36\ \mu s$. Since the value of T_{ig} was chosen ad hoc, these values for the transition length and time should not be construed as representative of SDT experiments; however, these values do agree well with the numerical predictions reported by Baer and Nunziato (1986) for the length (0.06 m) and time (33 μs) associated with DDT in porous HMX ($\phi_{2o} = 0.73$). The detonation wave, traveling at a faster speed, overtakes the compaction front at $t = 51\ \mu s$. Subsequently, a fully developed detonation wave having a reaction zone length of approximately 11 mm is formed. Following the detonation wave is a rarefaction wave in the gas which decreases the gas velocity from its value at the end of the reaction zone (2960 m/s) to that of the piston (100 m/s). The wave patterns are more easily seen in the gas density contours projected in the x- t plane given in Fig. 6.

Figures 7a-c show the numerically predicted variation in gas and solid pressure, gas and solid Mach number squared (relative to the wave), and solid volume fraction within the detonation wave at $t = 90\ \mu s$. Also plotted in these figures are the corresponding variations predicted by the steady-state theory of Powers et al. 1990b. Good agreement exists between the numerical predictions and the steady-state theory predictions. The wave structure consists of a single lead shock in the gas and an unshocked solid. Since the velocity of the gas relative to the wave is locally sonic at the end of the reaction zone, the wave is a two-phase equivalent of a single phase CJ detonation. The CJ wave speed predicted by the steady-state theory is 7499.8 m/s which agrees well with the numerical prediction of 7500 m/s. This speed is representative of experimentally observed CJ wave speeds in porous HMX.

6 Conclusions

In conclusion, a two-phase continuum model was numerically solved to predict detonation in a granulated material due to compression of the material by a moving piston. The model equations were solved using a high-resolution method which is based upon Godunov's method. The numerical method gave good results for a number of test problems in which known theoretical results were available for comparison. The existence of a SDT event leading to a fully resolved two-phase CJ detonation was demonstrated. Detailed comparisons between the numerical predictions and predictions given by a formal steady-state theory clearly identify that the detonation structure consists of a single lead shock in the gas and an unshocked solid. In this study, we emphasize the necessity of fully resolv-

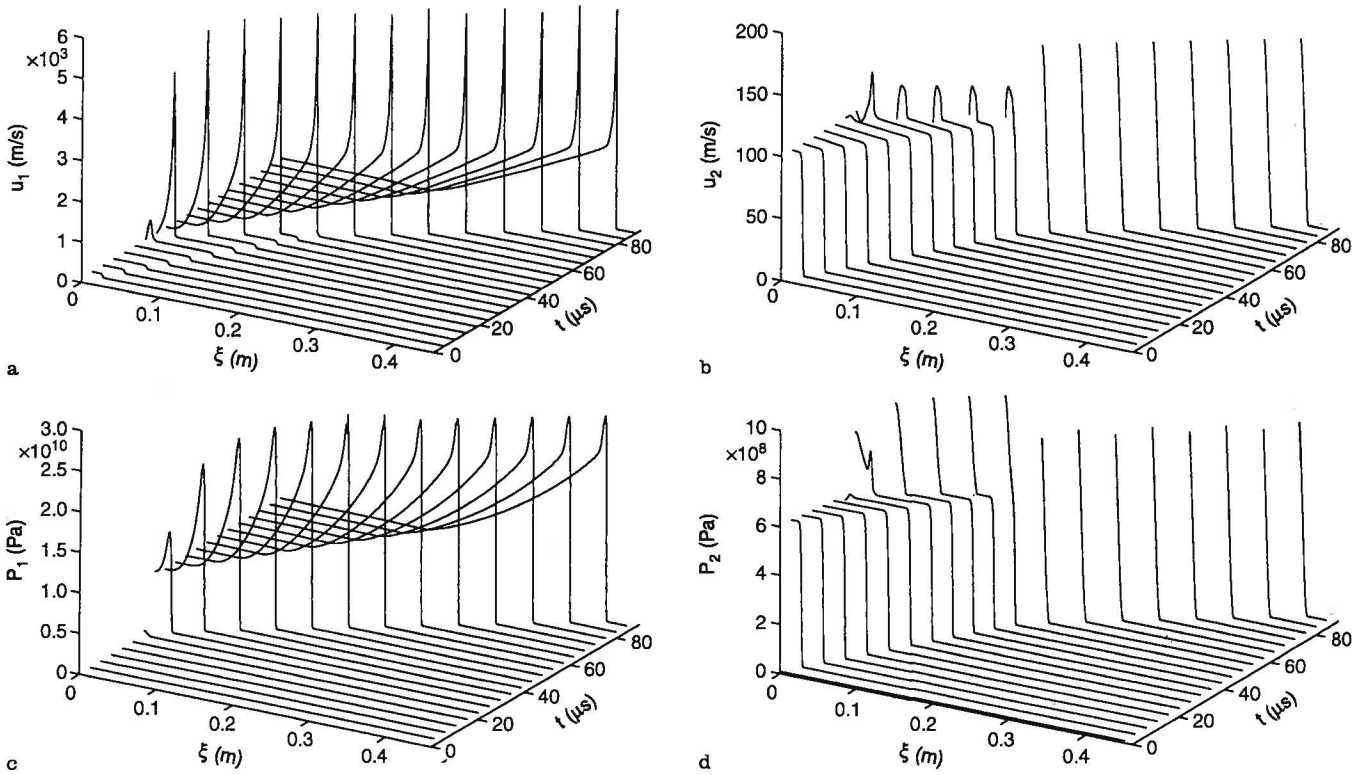

Fig. 5a–d. Numerical predictions for the detonation wave simulation: **a** gas velocity history, **b** solid velocity history, **c** gas pressure history, and **d** solid pressure history

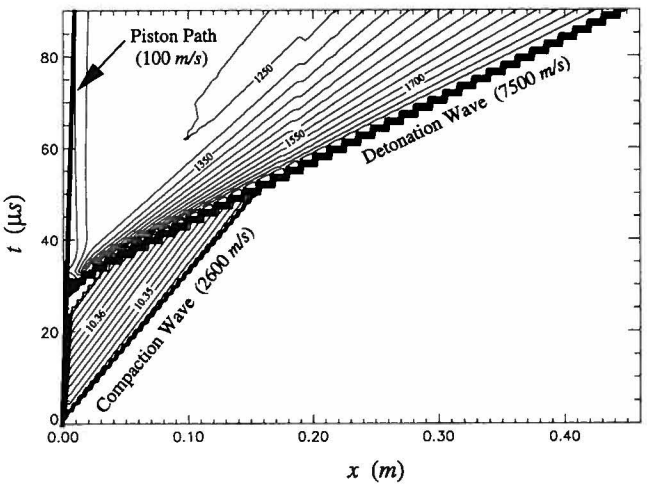

Fig. 6. Gas density (kg/m^3) contours in the (x, t)-plane for the detonation wave simulation

ing all spatial structures when numerically solving unsteady problems.

Since the focus of this study was on obtaining unsteady predictions which could be directly compared with previously published results for a steady two-phase CJ detonation, simple constitutive relations were used. Constitutive relations which are more representative of real physical systems can be easily incorporated into the model in order to obtain better predictive capabilities. Lastly, we note that additional work is needed to determine the influence of model singularities on both the analytical and computational solution.

Acknowledgements. This study was supported by the NASA Lewis Research Center, Cleveland, Ohio, USA, under Contract Number NASA-NCC3-325. Partial support for this study was given by Wright Laboratories, WL-MNMW, Eglin Air Force Base, Florida, USA.

Appendix A: Approximate solution of the Riemann problem

The two-phase Riemann problem is defined as the initial value problem

$$\frac{\partial \mathbf{q}}{\partial t} + \frac{\partial \mathbf{f}(\mathbf{q})}{\partial x} = 0, \qquad A.1$$

and

$$\mathbf{q}(x,0) = \begin{cases} \mathbf{q}_L, & \text{if } x < 0; \\ \mathbf{q}_R, & \text{if } x > 0, \end{cases} \qquad A.2$$

where $\mathbf{q}_L$ and $\mathbf{q}_R$ are constant states to the left and right of the initial discontinuity located at $x = 0$. To construct the approximate solution, the average quantities $\widetilde{\rho_1\phi_1}$, $\widetilde{u}_1$, $\widetilde{P_1\phi_1}$, $\widetilde{e}_1$, $\widetilde{F}_{1_{\rho 1\phi 1}}$, $\widetilde{F}_{1_{\phi 1}}$, $\widetilde{F}_{1_{e1}}$, $\widetilde{\rho_2\phi_2}$, $\widetilde{\phi}_2$, $\widetilde{u}_2$, $\widetilde{P_2\phi_2}$, $\widetilde{e}_2$, $\widetilde{F}_{2_{\rho 2\phi 2}}$, $\widetilde{F}_{2_{\phi 2}}$, $\widetilde{F}_{2_{e2}}$, and $\widetilde{n}$ [average quantities are denoted by $\widetilde{(\bullet)}$] are defined as

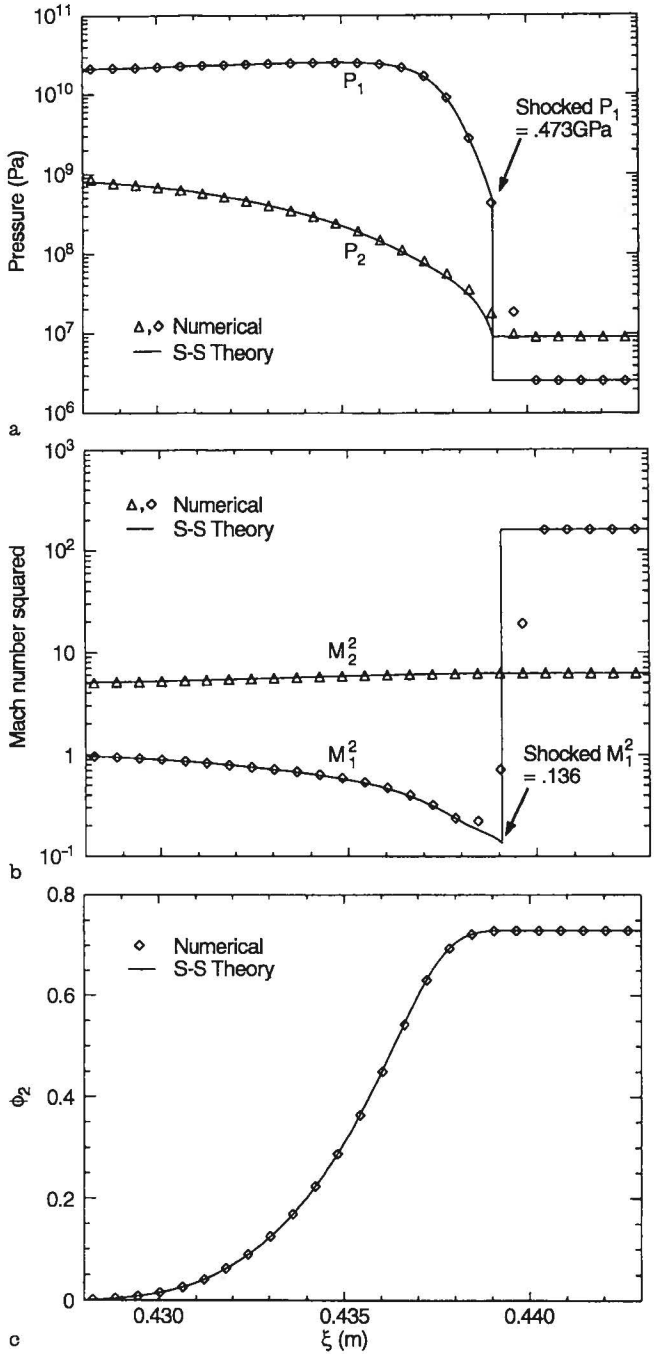

Fig. 7a–c. Comparison of the numerical and steady-state theory (S-S) prediction for detonation wave structure: **a** gas and solid pressure, **b** gas and solid Mach number squared (measured relative to wave), and **c** solid volume fraction

functions of $\mathbf{q}_L$ and $\mathbf{q}_R$ such that the following expressions are identically satisfied:

$$\Delta\mathbf{q} \equiv \mathbf{q}_R - \mathbf{q}_L = \sum_{k=1}^{8} \tilde{\alpha}^{(k)}\tilde{\mathbf{r}}^{(k)}, \qquad A.3$$

$$\Delta\mathbf{f} \equiv \mathbf{f}_R - \mathbf{f}_L = \sum_{k=1}^{8} \tilde{\lambda}^{(k)}\tilde{\alpha}^{(k)}\tilde{\mathbf{r}}^{(k)}. \qquad A.4$$

where

$$\tilde{\lambda}^{(1)} = \tilde{u}_1, \quad \tilde{\lambda}^{(2)} = \tilde{u}_1 + \tilde{c}_1, \quad \tilde{\lambda}^{(3)} = \tilde{u}_1 - \tilde{c}_1, \quad \tilde{\lambda}^{(4)} = \tilde{u}_2,$$

$$\tilde{\lambda}^{(5)} = \tilde{u}_2 + \tilde{c}_2, \quad \tilde{\lambda}^{(6)} = \tilde{u}_2 - \tilde{c}_2, \quad \tilde{\lambda}^{(7)} = \tilde{u}_2, \quad \tilde{\lambda}^{(8)} = \tilde{u}_2,$$

$$\tilde{\mathbf{r}}^{(1)} = \left[1,\ \tilde{u}_1,\ \tilde{H}_1 - \tilde{c}_1^2/\tilde{\Gamma}_1,\ 0,\ 0,\ 0,\ 0,\ 0\right]^T,$$

$$\tilde{\mathbf{r}}^{(2)} = \left[1,\ \tilde{u}_1 + \tilde{c}_1,\ \tilde{H}_1 + \tilde{u}_1\tilde{c}_1,\ 0,\ 0,\ 0,\ 0,\ 0\right]^T,$$

$$\tilde{\mathbf{r}}^{(3)} = \left[1,\ \tilde{u}_1 - \tilde{c}_1,\ \tilde{H}_1 - \tilde{u}_1\tilde{c}_1,\ 0,\ 0,\ 0,\ 0,\ 0\right]^T,$$

$$\tilde{\mathbf{r}}^{(4)} = \left[0,\ 0,\ 0,\ 1,\ \tilde{u}_2,\ \tilde{H}_2 - \tilde{c}_2^2/\tilde{\Gamma}_2,\ \tilde{\phi}_2,\ 0\right]^T,$$

$$\tilde{\mathbf{r}}^{(5)} = \left[0,\ 0,\ 0,\ 1,\ \tilde{u}_2 + \tilde{c}_2,\ \tilde{H}_2 + \tilde{u}_2\tilde{c}_2,\ \tilde{\phi}_2,\ \tilde{n}/\widetilde{\rho_2\phi_2}\right]^T,$$

$$\tilde{\mathbf{r}}^{(6)} = \left[0,\ 0,\ 0,\ 1,\ \tilde{u}_2 - \tilde{c}_2,\ \tilde{H}_2 - \tilde{u}_2\tilde{c}_2,\ \tilde{\phi}_2,\ \tilde{n}/\widetilde{\rho_2\phi_2}\right]^T,$$

$$\tilde{\mathbf{r}}^{(7)} = \left[-\frac{\tilde{F}_{1_{\phi 1}}}{\widetilde{\rho_2\phi_2}\left((\tilde{u}_2 - \tilde{u}_1)^2 - \tilde{c}_1^2\right)},\ -\frac{\tilde{F}_{1_{\phi 1}}\tilde{u}_2}{\widetilde{\rho_2\phi_2}\left((\tilde{u}_2 - \tilde{u}_1)^2 - \tilde{c}_1^2\right)},\right.$$
$$\left. -\frac{\tilde{F}_{1_{\phi 1}}\left(\tilde{H}_1 + \tilde{u}_1\tilde{u}_2 - \tilde{u}_1^2\right)}{\widetilde{\rho_2\phi_2}\left((\tilde{u}_2 - \tilde{u}_1)^2 - \tilde{c}_1^2\right)},\ 0,\ 0,\ -\frac{\tilde{F}_{2_{\phi 2}}}{\widetilde{\rho_2\phi_2}\tilde{\Gamma}_2},\ 1,\ 0\right]^T,$$

$$\tilde{\mathbf{r}}^{(8)} = [0,\ 0,\ 0,\ 0,\ 0,\ 0,\ 0,\ 1]^T,$$

$$\tilde{\alpha}^{(1)} = \Delta(\rho_1\phi_1) - \frac{1}{\tilde{c}_1^2}\Delta(P_1\phi_1) + \frac{\tilde{F}_{1_{\phi 1}}}{\tilde{c}_1^2}\Delta\phi_1,$$

$$\tilde{\alpha}^{(2)} = \frac{1}{2\tilde{c}_1^2}\Delta(P_1\phi_1) + \frac{\widetilde{\rho_1\phi_1}}{2\tilde{c}_1}\Delta u_1$$
$$-\left(\frac{\tilde{u}_2 - \tilde{u}_1}{\tilde{u}_2 - (\tilde{u}_1 + \tilde{c}_1)}\right)\frac{\tilde{F}_{1_{\phi 1}}}{2\tilde{c}_1^2}\Delta\phi_1,$$

$$\tilde{\alpha}^{(3)} = \frac{1}{2\tilde{c}_1^2}\Delta(P_1\phi_1) - \frac{\widetilde{\rho_1\phi_1}}{2\tilde{c}_1}\Delta u_1$$
$$-\left(\frac{\tilde{u}_2 - \tilde{u}_1}{\tilde{u}_2 - (\tilde{u}_1 - \tilde{c}_1)}\right)\frac{\tilde{F}_{1_{\phi 1}}}{2\tilde{c}_1^2}\Delta\phi_1,$$

$$\tilde{\alpha}^{(4)} = \Delta(\rho_2\phi_2) - \frac{1}{\tilde{c}_2^2}\Delta(P_2\phi_2),$$

$$\tilde{\alpha}^{(5)} = \frac{1}{2\tilde{c}_2^2}\Delta(P_2\phi_2) + \frac{\widetilde{\rho_2\phi_2}}{2\tilde{c}_2}\Delta u_2,$$

$$\tilde{\alpha}^{(6)} = \frac{1}{2\tilde{c}_2^2}\Delta(P_2\phi_2) - \frac{\widetilde{\rho_2\phi_2}}{2\tilde{c}_2}\Delta u_2,$$

$$\tilde{\alpha}^{(7)} = \widetilde{\rho_2\phi_2}\Delta\phi_2,$$

$$\tilde{\alpha}^{(8)} = \Delta n - \frac{\tilde{n}}{\widetilde{\rho_2\phi_2}\tilde{c}_2^2}\Delta(P_2\phi_2),$$

and $\tilde{c}_1$, $\tilde{c}_2$, $\tilde{H}_1$, $\tilde{H}_2$, $\tilde{\Gamma}_1$, and $\tilde{\Gamma}_2$ are defined by

$$\tilde{c}_1^2 \equiv \frac{\widetilde{P_1\phi_1}}{\widetilde{\rho_1\phi_1}^2}\tilde{F}_{1_{e1}} + \tilde{F}_{1_{\rho 1\phi 1}}, \quad \tilde{c}_2^2 \equiv \frac{\widetilde{P_2\phi_2}}{\widetilde{\rho_2\phi_2}^2}\tilde{F}_{2_{e2}} + \tilde{F}_{2_{\rho 2\phi 2}},$$

$$\widetilde{H}_1 \equiv \widetilde{e}_1 + \frac{\widetilde{u}_1^2}{2} + \frac{\widetilde{P_1\phi_1}}{\widetilde{\rho_1\phi_1}}, \quad \widetilde{H}_2 \equiv \widetilde{e}_2 + \frac{\widetilde{u}_2^2}{2} + \frac{\widetilde{P_2\phi_2}}{\widetilde{\rho_2\phi_2}},$$

$$\widetilde{\Gamma}_1 \equiv \frac{1}{\widetilde{\rho_1\phi_1}}\widetilde{F}_{1_{e1}}, \quad \widetilde{\Gamma}_2 \equiv \frac{1}{\widetilde{\rho_2\phi_2}}\widetilde{F}_{2_{e2}}.$$

In these expressions, $\Delta(\bullet) \equiv (\bullet)_R - (\bullet)_L$ is a difference operator, and $\widetilde{F}_{i_{\rho i\phi i}}$, $\widetilde{F}_{i_{\phi i}}$, and $\widetilde{F}_{i_{ei}}$ $(i = 1,2)$ are averages for the derivatives $\partial F_i/\partial(\rho_i\phi_i)$, $\partial F_i/\partial\phi_i$, and $\partial F_i/\partial e_i$ $(i = 1,2)$, respectively. The functional forms for the relationships $F_i(\rho_i\phi_i, \phi_i, e_i) = P_i\phi_i$ $(i = 1,2)$ are obtained using the equations of state for the gas and solid. The average quantities are defined by

$$\widetilde{\rho_i\phi_i} = \sqrt{\rho_{iL}\phi_{iL}\rho_{iR}\phi_{iR}},$$

$$\widetilde{u}_i = \frac{\sqrt{\rho_{iL}\phi_{iL}}u_{iL} + \sqrt{\rho_{iR}\phi_{iR}}u_{iR}}{\sqrt{\rho_{iL}\phi_{iL}} + \sqrt{\rho_{iR}\phi_{iR}}},$$

$$\widetilde{e}_i = \frac{\sqrt{\rho_{iL}\phi_{iL}}e_{iL} + \sqrt{\rho_{iR}\phi_{iR}}e_{iR}}{\sqrt{\rho_{iL}\phi_{iL}} + \sqrt{\rho_{iR}\phi_{iR}}},$$

$$\widetilde{H}_i = \frac{\sqrt{\rho_{iL}\phi_{iL}}H_{iL} + \sqrt{\rho_{iR}\phi_{iR}}H_{iR}}{\sqrt{\rho_{iL}\phi_{iL}} + \sqrt{\rho_{iR}\phi_{iR}}},$$

$$\widetilde{\phi}_2 = \frac{\sqrt{\rho_{2L}\phi_{2L}}\phi_{2L} + \sqrt{\rho_{2R}\phi_{2R}}\phi_{2R}}{\sqrt{\rho_{2L}\phi_{2L}} + \sqrt{\rho_{2R}\phi_{2R}}},$$

$$\widetilde{n} = \frac{\sqrt{\rho_{2L}\phi_{2L}}n_R + \sqrt{\rho_{2R}\phi_{2R}}n_L}{\sqrt{\rho_{2L}\phi_{2L}} + \sqrt{\rho_{2R}\phi_{2R}}},$$

$$\widetilde{F}_{i_{\rho i\phi i}} = \left\{ \frac{1}{4}\left[F_i(\rho_{iR}\phi_{iR}, \phi_{iR}, e_{iR}) + F_i(\rho_{iR}\phi_{iR}, \phi_{iR}, e_{iL}) + F_i(\rho_{iR}\phi_{iR}, \phi_{iL}, e_{iL}) + F_i(\rho_{iR}\phi_{iR}, \phi_{iL}, e_{iR})\right] - \frac{1}{4}\left[F_i(\rho_{iL}\phi_{iL}, \phi_{iR}, e_{iR}) + F_i(\rho_{iL}\phi_{iL}, \phi_{iL}, e_{iR}) + F_i(\rho_{iL}\phi_{iL}, \phi_{iR}, e_{iL}) + F_i(\rho_{iL}\phi_{iL}, \phi_{iL}, e_{iL})\right] \right\} / \Delta(\rho_i\phi_i), \quad \text{if } \Delta(\rho_i\phi_i) \neq 0, \qquad A.5$$

$$\widetilde{F}_{i_{\phi i}} = \left\{ \frac{1}{2}\left[F_i(\rho_{iR}\phi_{iR}, \phi_{iR}, e_{iR}) + F_i(\rho_{iL}\phi_{iL}, \phi_{iR}, e_{iL})\right] - \frac{1}{2}\left[F_i(\rho_{iR}\phi_{iR}, \phi_{iL}, e_{iR}) + F_i(\rho_{iL}\phi_{iL}, \phi_{iL}, e_{iL})\right] \right\} / \Delta\phi_i, \quad \text{if } \Delta\phi_i \neq 0, \qquad A.6$$

$$\widetilde{F}_{i_{ei}} = \left\{ \frac{1}{4}\left[F_i(\rho_{iR}\phi_{iR}, \phi_{iR}, e_{iR}) + F_i(\rho_{iL}\phi_{iL}, \phi_{iL}, e_{iR}) + F_i(\rho_{iR}\phi_{iR}, \phi_{iL}, e_{iR}) + F_i(\rho_{iL}\phi_{iL}, \phi_{iR}, e_{iR})\right] - \frac{1}{4}\left[F_i(\rho_{iR}\phi_{iR}, \phi_{iL}, e_{iL}) + F_i(\rho_{iR}\phi_{iR}, \phi_{iR}, e_{iL}) + F_i(\rho_{iL}\phi_{iL}, \phi_{iR}, e_{iL}) + F_i(\rho_{iL}\phi_{iL}, \phi_{iL}, e_{iL})\right] \right\} / \Delta e_i, \quad \text{if } \Delta e_i \neq 0. \qquad A.7$$

For $\Delta(\rho_i\phi_i) = 0$, $\Delta\phi_i = 0$ or $\Delta e_i = 0$ $(i = 1,2)$, we take the appropriate limits of Eqs. (A.5-A.7) [i.e., as $\Delta(\rho_i\phi_i) \to 0$, $\Delta\phi_i \to 0$, and $\Delta e_i \to 0$, respectively] to obtain the following expressions:

$$\widetilde{F}_{i_{\rho i\phi i}} = \frac{1}{4}\left[\frac{\partial F_i}{\partial(\rho_i\phi_i)}(\rho_i\phi_i, \phi_{iR}, e_{iR}) + \frac{\partial F_i}{\partial(\rho_i\phi_i)}(\rho_i\phi_i, \phi_{iR}, e_{iL}) + \frac{\partial F_i}{\partial(\rho_i\phi_i)}(\rho_i\phi_i, \phi_{iL}, e_{iR}) + \frac{\partial F_i}{\partial(\rho_i\phi_i)}(\rho_i\phi_i, \phi_{iL}, e_{iL})\right], \quad \text{if } \Delta(\rho_i\phi_i) = 0,$$

$$\widetilde{F}_{i_{\phi i}} = \frac{1}{2}\left[\frac{\partial F_i}{\partial \rho_i}(\rho_{iR}\phi_{iR}, \phi_i, e_{iR}) + \frac{\partial F_i}{\partial \rho_i}(\rho_{iL}\phi_{iL}, \phi_i, e_{iL})\right], \quad \text{if } \Delta\phi_i = 0,$$

$$\widetilde{F}_{i_{ei}} = \frac{1}{4}\left[\frac{\partial F_i}{\partial e_i}(\rho_{iR}\phi_{iR}, \phi_{iR}, e_i) + \frac{\partial F_i}{\partial e_i}(\rho_{iR}\phi_{iR}, \phi_{iL}, e_i) + \frac{\partial F_i}{\partial e_i}(\rho_{iL}\phi_{iL}, \phi_{iR}, e_i) + \frac{\partial F_i}{\partial e_i}(\rho_{iL}\phi_{iL}, \phi_{iL}, e_i)\right], \quad \text{if } \Delta e_i = 0.$$

In the solution outlined here, the average quantities $\widetilde{\lambda}^{(k)}$ $(k = 1, \ldots, 8)$ are approximations for the propagation speeds of the waves associated with the solution of the Riemann problem, and the average quantities $\widetilde{\alpha}^{(k)}\widetilde{\mathbf{r}}^{(k)}$ are approximations for the jump in the state of the system across these waves. The approximate solution is constructed such that as $\mathbf{q}_R - \mathbf{q}_L \to 0$, it reduces to the exact solution of the linearized Riemann problem [i.e., for $\mathbf{q}_R - \mathbf{q}_L = O(\epsilon)$, ϵ small]. Furthermore, Eq. (A.4) guarantees that the numerical scheme is conservative since, across the k^{th} wave, we require $\lambda^{(k)} = \delta\mathbf{f}^{(k)}/\delta\mathbf{q}^{(k)}$, where $\delta\mathbf{q}^{(k)} \equiv \widetilde{\alpha}^{(k)}\widetilde{\mathbf{r}}^{(k)}$ and $\delta\mathbf{f}^{(k)} \equiv \widetilde{\lambda}^{(k)}\widetilde{\alpha}^{(k)}\widetilde{\mathbf{r}}^{(k)}$ are jumps in the conserved variables and the fluxes across the k^{th} wave, respectively. Details concerning the derivation of the approximate Riemann solution outlined here are given by Gonthier (1996).

References

Baer MR, Nunziato JW (1986) A two-phase mixture theory for the deflagration to detonation transition (DDT) in reactive granular materials. Int J Multiphase Flow 12:861-889

Baer MR, Gross RJ, Nunziato JW, and Igel EA (1986) An experimental and theoretical study of deflagration-to-detonation transition (DDT) in the granular explosive, CP. Combust and Flame 65:15-30

Bell JB, Colella P, Trangenstein JA (1989) Higher order Godunov methods for general systems of hyperbolic conservation laws. J Comp Phys 82:362-397

Bement LJ, Schimmel ML (1988) Investigation of Super*Zip separation joint. NASA Technical Memorandum 4031

Bernecker RR, Price D (1974a) Studies in the transition from deflagration to detonation in granular explosives. I. Experimental arrangement and behavior of explosives which fail to exhibit detonation. Combust and Flame 22:111-118

Bernecker RR, Price D (1974b) Studies in the transition from deflagration to detonation in granular explosives. II. Transitional characteristics and mechanisms observed in 91/9 RDX wax. Combust and Flame 22:119-129

Butler PB, Krier H (1986) Analysis of deflagration to detonation transition in high- energy solid propellants. Combust and Flame 63:31-48

Chakravarthy SR, Osher S (1985) Computing with high-resolution upwind schemes for hyperbolic equations. In: Lectures in Applied Mathematics, American Mathematical Society (22), pp 57-86

Embid P, Baer M (1992) Mathematical analysis of a two-phase continuum mixture theory. Continuum Mech Thermodyn 4:279-312

Embid PF, Majda AJ (1992) An asymptotic theory for hot spot formation and transition to detonation for reactive granular materials. Combust and Flame 89:17-36

Embid P, Hunter J, Majda A (1992) Simplified asymptotic equations for the transition to detonation in reactive granular materials. SIAM J Appl Math 52:1199- 1237

Fickett W, Davis WC (1979) Detonation. University of California Press

Glaister P (1988) An approximate linearised Riemann solver for the Euler equations for real gases. J Comp Phys 74:382-408

Gonthier KA (1996) PhD dissertation. Dept of Aero and Mech Engr, University of Notre Dame, Notre Dame, IN

Osher S, Solomon F (1982) Upwind difference schemes for hyperbolic systems of conservation laws. Math Comp 38:339-374

Osher S (1984) Riemann solvers, the entropy condition and difference approximations. SIAM J Numer Anal 21:217-235

Powers JM, Stewart DS, Krier H (1989) Analysis of steady compaction waves in porous materials. J Appl Mech 56:15-24

Powers JM, Stewart DS, Krier H (1990a) Theory of two-phase detonation – part I: modeling. Combust and Flame 80:264-279

Powers JM, Stewart DS, Krier H (1990b) Theory of two-phase detonation – part II: structure. Combust and Flame 80:280-303

Roe PL (1981) Approximate Riemann solvers, parameter vectors, and difference schemes. J Comp Phys 43:357-372

Sandusky HW, Liddiard TP (1985) Dynamic compaction of porous beds. Naval Surface Weapons Center NSWC TR 83-246

Saurel R, Larini M, and Loraud JC (1992) Ignition and growth of a detonation by a high energy plasma. Shock Waves 2:19-29

Smirnov NN, and Tyurnikov MV (1994) A study of deflagration and detonation in multiphase hydrocarbon-air mixtures. Combust and Flame 96:130-140

Stewart DS, Asay BW, and Prasad K (1994) Simplified modeling of transition to detonation in porous energetic materials. Phys Fluids 6(7):2513-2533

Strang G (1968) On the construction and comparison of difference schemes. SIAM J Num Anal 5:506-517

Toro EF (1989) A fast Riemann solver with constant covolume applied to the random choice method. Int J for Numer Methods Fluids 9:1145-1164

Whitham GB (1974) Linear and nonlinear waves. John Wiley, New York

Zauderer E (1989) Partial differential equations of applied mathematics. Wiley, New York